

# Multi-messenger High-Energy Signatures of Decaying Dark Matter and the Effect of Background Light

B. Skrzypek,<sup>a,1</sup> M. Chianese,<sup>b,c</sup> C. A. Argüelles<sup>a</sup>

<sup>a</sup>Department of Physics & Laboratory for Particle Physics and Cosmology,  
Harvard University, Cambridge, MA 02138, USA

<sup>b</sup>Dipartimento di Fisica “Ettore Pancini”, Università degli studi di Napoli “Federico II”, Complesso Univ. Monte S. Angelo, I-80126 Napoli, Italy

<sup>c</sup>INFN - Sezione di Napoli, Complesso Univ. Monte S. Angelo, I-80126 Napoli, Italy

E-mail: [bskrzypek@g.harvard.edu](mailto:bskrzypek@g.harvard.edu), [chianese@na.infn.it](mailto:chianese@na.infn.it), [carguelles@fas.harvard.edu](mailto:carguelles@fas.harvard.edu)

**Abstract.** The IceCube Neutrino Observatory at the South Pole has measured astrophysical neutrinos using through-going and starting events in the TeV to PeV energy range. The origin of these astrophysical neutrinos is still largely unresolved, and among their potential sources could be dark matter decay. Measurements of the astrophysical flux using muon neutrinos are in slight tension with starting event measurements. This tension is driven by an excess observed in the energy range of 40-200 TeV with respect to the through-going expectation. Previous works have considered the possibility that this excess may be due to heavy dark matter decay and have placed constraints using gamma-ray and neutrino data. However, these constraints are not without caveats since they rely on the modeling of the astrophysical neutrino flux and the sources of gamma-ray emission. In this work, we derive background-agnostic galactic and extragalactic constraints on decaying dark matter by considering Tibet AS<sub>γ</sub> data, Fermi-LAT diffuse data, and the IceCube high-energy starting event sample. For the gamma-ray limits, we investigate the uncertainties on secondary emission from electromagnetic cascades during propagation arising from the unknown intensity of the extragalactic background light. We find that such uncertainties amount to a variation of up to  $\sim 55\%$  in the gamma-ray limits derived with extragalactic data. Our results imply that a significant fraction of the astrophysical neutrino flux could be due to dark matter and that ruling it out depends on the assumptions on the gamma-ray and neutrino background. The latter depends on the yet unidentified sources.

---

<sup>1</sup>Corresponding author.

---

## Contents

<b>1</b>	<b>Introduction</b>	<b>1</b>
<b>2</b>	<b>Heavy Dark Matter Decay and its Signatures</b>	<b>2</b>
<b>3</b>	<b>The Extragalactic Background Light</b>	<b>5</b>
<b>4</b>	<b>Analysis and Results</b>	<b>9</b>
<b>5</b>	<b>Conclusions</b>	<b>13</b>
<b>A</b>	<b>Simulation Details</b>	<b>19</b>
	A.1 Position Reweighting	19
	A.2 Energy Reweighting	20
<b>B</b>	<b>Spectra of Photons Arriving at Earth</b>	<b>20</b>

---

## 1 Introduction

The measurement of High-Energy Starting Event (HESE) neutrinos in the TeV-PeV range by the IceCube Neutrino Observatory has introduced new questions in connection to their origin and properties [1–3]. These open questions have the possibility of being answered through multi-messenger efforts in astroparticle physics [4, 5]. In particular, the excess observed in the 7.5-year HESE sample, with its sensitivity to the Galactic center and, generally, to the entire sky, cannot originate entirely from the atmospheric neutrino background, nor does it lend itself to a simple astrophysical power-law distribution given the observations in other channels [6]. Instead, a two-component power-law spectrum, the nature of which is in question, is favored by the data. Moreover, the modeling of this astrophysical contribution is yet to be determined. However, it is well-known that the production mechanisms involved in giving rise to highly energetic astrophysical neutrinos, namely the decay of charged pions originating from hadronic [7, 8] and photohadronic [9, 10] interactions, also produce coincident gamma-rays at the source. Most notably, this coincident emission was confirmed by the multi-messenger observation of the flaring blazar TXS 0506+056 [11–13].

However, the high level of gamma-ray suppression from astrophysical sources along with tensions among current IceCube datasets in measurements of the astrophysical spectrum make it difficult to characterize the nature of the source of these ultra-high-energy neutrinos. With the assumption of a single unbroken power-law flux, the 10-year through-going (TG) muon sample, which is sensitive to neutrinos coming only from the Northern sky and with energies larger than 15 TeV, measures a spectral index of  $2.37^{+0.09}_{-0.09}$  [14]. This measurement is consistent with theoretical predictions of neutrinos originating from photohadronic processes [15] and with measurements of TXS 0506+056. On the other hand, HESE, with sensitivity to the entire sky and to energies starting from 20 TeV, obtains a spectral index  $2.87^{+0.20}_{-0.19}$  [6]. This suggests that there could be an additional component contributing to the neutrino flux that HESE observes that dominates at lower energies and comes from [16–27].

Given this observation, heavy dark matter has been proposed as a potential source of the neutrinos in the HESE sample [28–37] (see Ref.s [38–40] for the IceCube analyses). Heavy

decaying dark matter also gives rise to gamma-rays [41–43] which have been searched with gamma-ray telescopes. Diffuse gamma-ray data places strong constraints on the dark matter lifetime for various decay channels, and these largely disfavor the dark matter hypothesis for IceCube’s observations [44–54]. In order to properly constrain the size of the dark matter contribution in HESE, we need to establish the robustness of these gamma-ray bounds.

In this work, we elaborate on previous dark matter decay results by considering the impact that the Extragalactic Background Light (EBL) could have on the predicted gamma-ray spectrum from dark matter. The presence of different EBL models is due to the fact that direct measurements are difficult and involve many uncertainties and tensions among observations, such as the disagreement between near-IR data and observations of very high-energy photons from extragalactic sources. As a result, there are various techniques used to model the EBL [55–63], some of which are based on local galaxy properties and others which are phenomenological approaches targeting a larger redshift range. We simulate the propagation of photons, electrons, and positrons using three different models of the EBL distribution, and we compute the resulting gamma-ray spectra at Earth predicted by dark matter decay. From there, we compare the fluxes to Tibet AS $_{\gamma}$  data [64] and Fermi-LAT diffuse measurements of the isotropic diffuse gamma-ray background (IGRB) [65], and we obtain lower bounds on the dark matter lifetime among the different EBL models that could have significant implications for existing limits.

The paper is organized as follows. In Section 2, we discuss the high-energy neutrino and gamma-ray signatures of dark matter decay. In Section 3, we study the impact of the EBL uncertainties in the propagation of gamma-rays. In Section 4, we describe our analyses on neutrino and gamma-ray data sets and present our results. Finally, in Section 5 we conclude.

## 2 Heavy Dark Matter Decay and its Signatures

Generally, models of heavy dark matter allow for decay modes where the final products are Standard Model particle-antiparticle pairs. In all the decay modes, neutrinos and gamma-rays are directly produced through the electroweak and hadronic cascades which immediately follow the decay as well as the electroweak radiative corrections which become relevant for dark matter masses larger than 100 GeV [41, 43]. Together, these determine the neutrino and gamma-ray differential energy spectra, which we denote as  $dN_i/dE$  with  $i = \nu, \gamma$ . This is used as the first input to compute the observed fluxes at Earth.

Because of their nature, neutrinos injected by dark matter decay reach the Earth unperturbed, barring effects on their final state flavor configuration due to neutrino oscillations. Therefore, the neutrino flux at the Earth can be easily calculated from the initial neutrino differential spectrum. We can characterize dark matter sources as either galactic (G) or extragalactic (EG) in nature, and thus the final differential neutrino flux can be broken down into galactic and extragalactic contributions, namely

$$\frac{d\phi_{\nu}}{dE_{\nu}d\Omega} = \frac{d\phi_{\nu}^G}{dE_{\nu}d\Omega} + \frac{d\phi_{\nu}^{EG}}{dE_{\nu}d\Omega}, \quad (2.1)$$

where  $E_{\nu}$  denotes the neutrino energy and  $\Omega$  denotes the solid angle.

For the galactic contribution, we assume a generalized Navarro-Frank-White (NFW) dark matter profile density, which takes the form

$$\rho(r(s, \ell, b)) = \rho_s \left( \frac{r}{R_s} \right)^{-\gamma} \left( 1 + \frac{r}{R_s} \right)^{-3+\gamma}, \quad (2.2)$$

$$r(s, \ell, b) = \sqrt{s^2 + R_\odot^2 - 2sR_\odot \cos \ell \cos b}, \quad (2.3)$$

where  $b$  and  $\ell$  are the galactic coordinates. Here, we fix the parameters  $\gamma = 0.4$ ,  $\rho_s \sim 0.57 \text{ GeV/cm}^3$ ,  $R_\odot = 8.5 \text{ kpc}$ , and  $R_s \sim 83.24 \text{ kpc}$  by minimizing the chi-squared distributions obtained in [66].<sup>1</sup> Varying these parameters within their allow ranges does not significantly affect our results. This is because, in the case of decaying dark matter, the choice of galactic profile parameters and their corresponding uncertainties does not carry as much weight as it does for the case of annihilating dark matter, where the flux is proportional to the square of the density rather than just a single power of the density. Hence, the galactic neutrino flux can be computed as

$$\frac{d\phi_\nu^G}{dE_\nu d\Omega} = \frac{1}{4\pi m_{\text{DM}} \tau_{\text{DM}}} \frac{dN_\nu}{dE_\nu} \int ds \rho(s, \ell, b), \quad (2.4)$$

where  $m_{\text{DM}}$  and  $\tau_{\text{DM}}$  are the dark matter mass and lifetime, respectively. The differential neutrino spectrum includes neutrino and anti-neutrinos of all the three flavours and is computed by means of the `HDMSpectra` code [43].

The extragalactic dark matter component, on the other hand, is generally taken to be isotropic. The resulting extragalactic flux can be written as an integral over cosmological distances parametrized by redshift  $z$ , where we also need to account for the redshift in the neutrino energies. This amounts to a difference between the fluxes at production and detection. The corresponding neutrino flux at detection is:

$$\frac{d\phi_\nu^{\text{EG}}}{dE_\nu d\Omega} = \frac{\Omega_{\text{DM}} \rho_{\text{cr}}}{4\pi m_{\text{DM}} \tau_{\text{DM}}} \int \frac{dz}{H(z)} \left. \frac{dN_\nu}{dE_\nu} \right|_{E'_\nu = E_\nu(1+z)}, \quad (2.5)$$

where  $H(z) = H_0 \sqrt{\Omega_\Lambda + \Omega_m(1+z)^3}$  is the Hubble parameter and  $\rho_{\text{cr}}$  is the critical density of the Universe [67]. Throughout this work we set the cosmological parameters to be:  $\Omega_{\text{DM}} = 0.23$ ,  $\Omega_\Lambda = 0.77$ ,  $\Omega_m = 0.27$ , and  $H_0 = 67.7 \text{ km/s/Mpc}$ . These are not the most recent values of the Planck parameters, but small changes to these should result in neither large changes to our conclusions nor changes to the final limits that we obtain.

Unlike in the case of neutrinos, the flux of gamma-rays produced from dark matter decay is heavily impacted by the intermediate interactions that arise from the subsequent propagation of photons and charged particles to Earth. At high energies, photons interact with background radiation and produce electron-positron pairs, preventing a subset of gamma-rays from reaching the Earth. Primary gamma-rays therefore experience an attenuation which is encoded in the optical depth,  $\tau_{\gamma\gamma}$ , which is a quantity that depends on the photon energy as well as the distance from the source to Earth. Additionally, electrons and positrons undergo interactions such as Inverse Compton scattering with background photons, bremsstrahlung, and synchrotron radiation in the galactic and intergalactic magnetic field. These processes can occur several times over the course of propagation, thus developing electromagnetic cascades that result in a secondary flux of low-energy photons at Earth [68–72]. Hence, the final photon flux is a combination of galactic and extragalactic components, each of which receives a prompt and two secondary (sec.) contribution from primary photon and electrons:

$$\frac{d\phi_\gamma^\alpha}{dE_\gamma d\Omega} = \frac{d\phi_\gamma^{\text{prompt}}}{dE_\gamma d\Omega} + \frac{d\phi_\gamma^{\text{sec.}}}{dE_\gamma d\Omega} + \frac{d\phi_{e^\pm \rightarrow \gamma}^{\text{sec.}}}{dE_\gamma d\Omega} \quad \text{with } \alpha = \text{G or EG}, \quad (2.6)$$

<sup>1</sup>The chi-squared distribution given in [66] when profiled over the other parameters is very flat in  $R_s$  allowing values that range from 5 to 90 kpc. Another typical value that is chosen in the literature for  $R_s$  is approximately 24 kpc. The resulting column densities that are relevant for this work are not significantly affected by this choice.

where  $\phi_\gamma^{\text{prompt}}$  and  $\phi_{\gamma\rightarrow\gamma}^{\text{sec.}}$  are the unscattered and cascaded components of the primary gamma-ray flux  $\phi_\gamma^{\text{prompt}}$  respectively, while  $\phi_{e^\pm\rightarrow\gamma}^{\text{sec.}}$  is the contribution of gamma-rays from the interactions of the primary electrons.

The prompt gamma-ray flux can be similarly computed as Eq. (2.4) and Eq. (2.5) up to an attenuation factor also known as gamma-ray opacity,  $e^{-\tau_\gamma}$ . As will be discussed in Section 3, the opacity is computed from the photon energy distribution in the background field and the cross sections for each of the relevant processes. As a result, changes in our modeling of the background radiation result in differences in the observed prompt flux. Although the spectrum of electromagnetic cascades initiated by primary photons and electrons approaches a nearly universal form consisting of two power-law components:  $E_\gamma^{-1.5}$  for  $E_\gamma \leq \mathcal{O}(0.1 \text{ GeV})$ , and  $E_\gamma^{-1.9}$  for  $E_\gamma \leq \mathcal{O}(10^5 \text{ GeV})$  [72], different spectral energy distributions of the background radiation can still slightly alter the universal gamma-ray spectrum. The secondary gamma-ray flux can typically be computed by means of analytical and numerical approaches [72–77].

In this analysis, we use the public simulation software **CRPropa** [78, 79] to calculate the gamma-ray flux in Eq. (2.6). This code allows us to propagate photons and electrons over galactic and extragalactic distances with different EBL models. In principle, such calculations require as input the differential spectrum of primary photons and electrons directly injected by dark matter decay as well as the dark matter distribution on galactic and extragalactic scales. However, these calculations are computationally intensive, making the injection of different dark matter spectra impractical. To overcome this difficulty we have developed a reweighting scheme that allows us to use a benchmark **CRPropa** simulation and transform it to yield the appropriate result. Our benchmark simulation assumes a single unbroken power-law in energy that ranges from the minimum energy of interest to the largest dark matter mass considered. To be able to efficiently reweight the galactic and extragalactic components, we produce two Monte Carlo data sets with the benchmark energy spectra which are then used to compute the galactic and extragalactic dark matter flux components. In both cases, we inject a spectrum that is uniformly distributed over a sphere, where the radii are 100 kpc and 10 Gpc for the galactic and extragalactic sets, respectively. Further details of the simulation and our Monte Carlo reweighting procedure can be found in Appendix A.

In Fig. 1, we show the different gamma-ray components described in this section, in the case of dark matter decaying to  $b\bar{b}$  with a mass of 1 PeV and a lifetime of  $10^{27}$  s. The dashed lines are the initial spectra corresponding to the gamma-rays and electron/positron final-states, directly emitted by dark matter particles. Additionally, the solid lines represent the final gamma-ray spectra that we see at Earth after propagation. Among these, we note that the galactic dark matter gamma-ray spectrum (red shades of color) is heavily dominated by an overall attenuation from the initial spectrum, whereas secondary production is merely a subleading effect. This is consistent with the fact that the short propagation scales contribute to the significant suppression of gamma-ray cascade production. In contrast, there is visible secondary production in the extragalactic components (blue shades of color), seen as the abundance at lower energies, indicating that secondary production is the dominant mechanism giving rise to gamma-rays from extragalactic dark matter decay. Alluding to the main goal of this work, secondary production is heavily informed by the spectral energy distribution of the background radiation, suggesting that the extragalactic component will see greater effects from changes in the modeling of that background. We elaborate on this point in the next section.

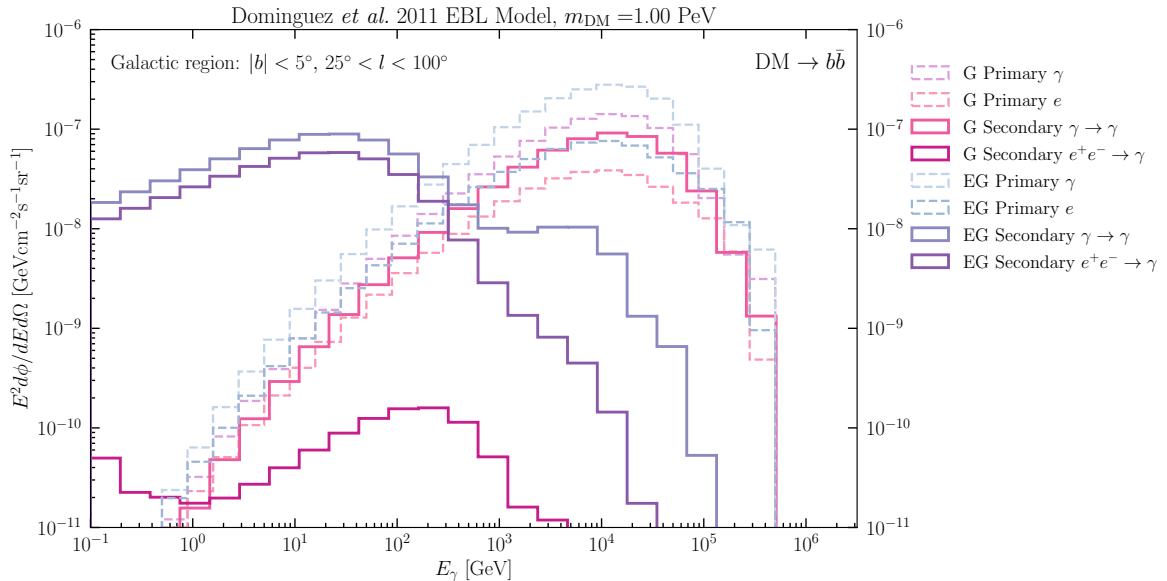


**Figure 1:** The different gamma-ray components from galactic (G) and extragalactic (EG) sources for  $m_{\text{DM}} = 1$  PeV and  $\tau_{\text{DM}} = 10^{27}$  s. The dashed lines show the initial spectra for gamma-rays and  $e^+e^-$  resulting from  $\text{DM} \rightarrow b\bar{b}$  decay as they appear at the source prior to propagation. The solid lines are the final spectra at Earth we obtain using `CRPropa` simulations and subsequently applying our reweighting procedure (see Appendix A). We fix the EBL spectrum according to the Dominguez *et al.* model [55].

### 3 The Extragalactic Background Light

The EBL, along with the Cosmic Microwave Background (CMB), is the primary target for the  $\gamma - \gamma$  and  $e - \gamma$  interactions. It is produced by the radiation emitted by all the galaxies over the history of cosmic evolution. Unlike the well-measured CMB spectrum, however, there are limited ways to measure the EBL directly, and therefore it has significant uncertainties. In particular, there are no direct measurements of the EBL below  $\sim 100 \mu\text{m}$  because of radiation from Zodiacal light coming from interplanetary dust radiation, which is about two orders of magnitude larger than the EBL flux [56]. Collective limits obtained from direct and indirect methods show that the EBL has a two-peak structure in the spectral energy distribution from the ultraviolet and the far-infrared [80, 81]. However, the incomplete information surrounding the structure of EBL has led to the development of different models, which use different methods for estimating its structure [55–63]. This uncertainty propagates down to the prediction of gamma-ray fluxes from distant point-like sources [82, 83] and the aggregated diffuse distribution of sources as is the case of dark matter. In this analysis we consider the following benchmark models provided by Dominguez *et al.* [55] and Stecker *et al.* [56]. We select these as benchmark models for our analysis in part because they are motivated by observational uncertainties in the EBL and because they are supported by constraints from data.

The Dominguez *et al.* 2011 model [55] is an *ab initio* evolution model that begins with initial conditions and evolves forward in time by using semi-analytical models of galaxy formation. The authors adopt a novel method whereby they use the observed evolution of the rest-frame  $K$ -band galaxy luminosity function along with galaxy SED functions, which are based on a sample of 6000 galaxies in the range of 0.2 to 1.0 in redshift from the All-wavelength

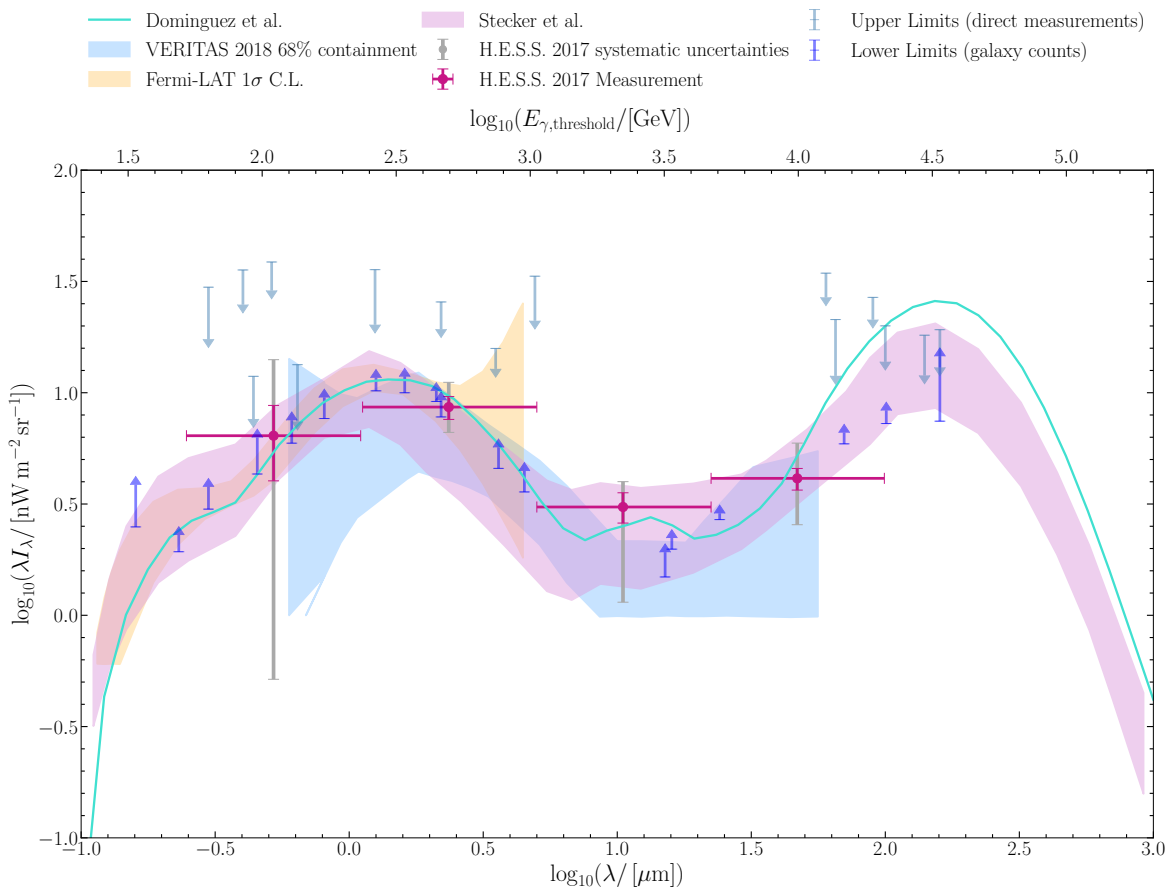


**Figure 2:** Spectral energy distributions (SEDs) at  $z = 0$  predicted by the EBL models that we consider. Shown in purple is the 68% confidence band obtained from Stecker *et al.* Minimal and Maximal models [56], and the cyan curve is the SED computed by Dominguez *et al.* [55]. The bottom axis gives the wavelength of the target photons, while the top axis recasts this in terms of the minimum (threshold) energy  $E_{\gamma,\text{threshold}}$  required by an incoming photon to produce an electron-positron pair. We also show several observational results for comparison, including direct constrains on the EBL in the form of upper and lower limits from direct measurements [84] and galaxy counts [85]. In addition, we show the most recent data provided by VERITAS [86] and H.E.S.S. [87]., and the  $1\sigma$  confidence level from Fermi-LAT based on reconstructed cosmic emissivity [81]. Note that the lower cutoff seen in the VERITAS band is artificial.

Extended Groth Strip International Survey (AEGIS). In addition to this, the authors also use their own estimates of the SED fractions of star-forming galaxies, starburst galaxies, and active galactic nuclei (AGN) galaxies. From this, the authors are able to extrapolate the evolution of the luminosity densities from the UV to the IR range in target wavelengths. Comparing their results to observations, they conclude with the claim that the EBL is well-constrained in the UV to mid-IR range, but that additional constraints from IR and gamma-ray astronomy are needed in order to account for uncertainties in the far-IR region.

On the other hand, the Stecker *et al.* 2016 model [56] is a backward evolution model that begins with a present-day luminosity function and extrapolates backwards in time. To

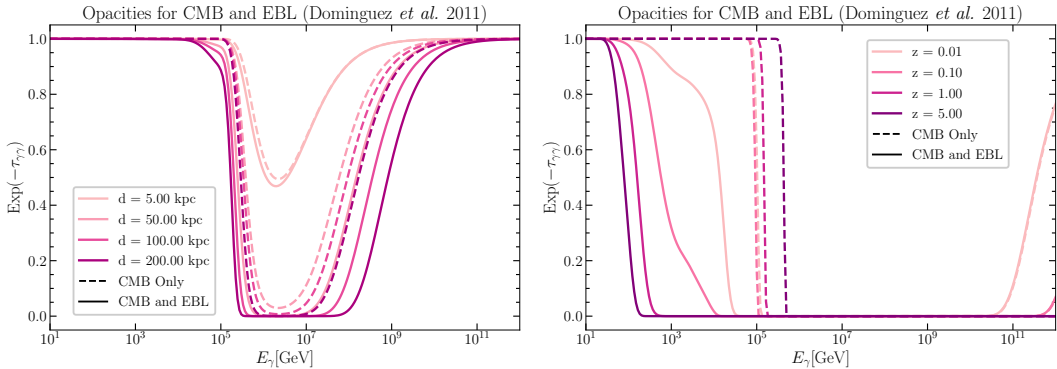


**Figure 3:** Opacities calculated for sources at distances on galactic (left) and extragalactic (right) scales. The solid (dashed) lines correspond to optical depths calculated including the CMB with (without) the EBL contribution for the Dominguez *et al.* model [55].

accomplish this, they use recent deep galaxy survey data at infrared wavelengths, which is where galaxy emission arises from dust re-radiation. In addition to this, the authors use the gamma-ray opacity from photons in the 2.7 K cosmic background radiation to extend their results to energies beyond the TeV scale. For wavelengths in the range  $5 \mu\text{m}$  to  $850 \mu\text{m}$ , they use empirical data from the Spitzer telescope, the Herschel telescope, the Planck space telescope, and observations from the Atacama Large Millimeter Array (ALMA) and the Balloon-borne Large Aperture Submillimeter Telescope (BLAST). Since the authors use only empirical data, their results are model independent, thereby taking into consideration the observational uncertainties of the EBL without additional assumptions about the evolution of galaxy luminosity functions, star formation rates, or galaxy evolution. The resulting uncertainties on the EBL that they present therefore reflect the observationally determined errors that they use. When performing their fit to observational data, they assume that the gamma-ray opacity arises entirely from pair-production interactions with the EBL. Moreover, they make use of luminosity densities (LDs), which are obtained by integrating fits to observationally determined luminosity functions, to determine photon densities. This includes fits to broken power-law functions describing galaxies as well as a double power-law fitting function. In order to compute the 68% limits on the LDs, the authors perform an upper and lower limit power-law function fit in the region representing the rate of decline of the LDs at redshifts beyond the peak of star formation. In computing the upper limit, they assume a  $(1+z)^{-2}$  decline in LD, while for the lower limit, they use a steeper decline of  $(1+z)^{-4}$ .

These models predict significantly different photon number densities, encompassing the ranges allowed by uncertainties in the EBL. Fig. 2 shows the spectral energy distributions predicted by the Dominguez *et al.* and Stecker *et al.* models as well as data points from various observations and experiments. These target wavelengths are in one-to-one correspondence with the minimum incoming photon energy required to produce electron-positron pairs, resulting in absorption and the development of an electromagnetic cascade. We show this quantity, which we call  $E_{\gamma,\text{threshold}}$ , on the top axis. In terms of the target wavelength, this is given by  $E_{\gamma,\text{threshold}} \sim m_e^2 \lambda$ , where  $m_e$  is the electron mass and  $\lambda$  is the target wavelength.

To understand the impact of the EBL in the gamma-ray fluxes that arrive at Earth, we can analytically calculate the optical depth  $\tau_{\gamma\gamma}$ . This quantity defines the gamma-ray opacity,  $e^{-\tau_{\gamma\gamma}}$ , which describes the absorption of high-energy gamma-rays due to  $\gamma - \gamma$  interactions.

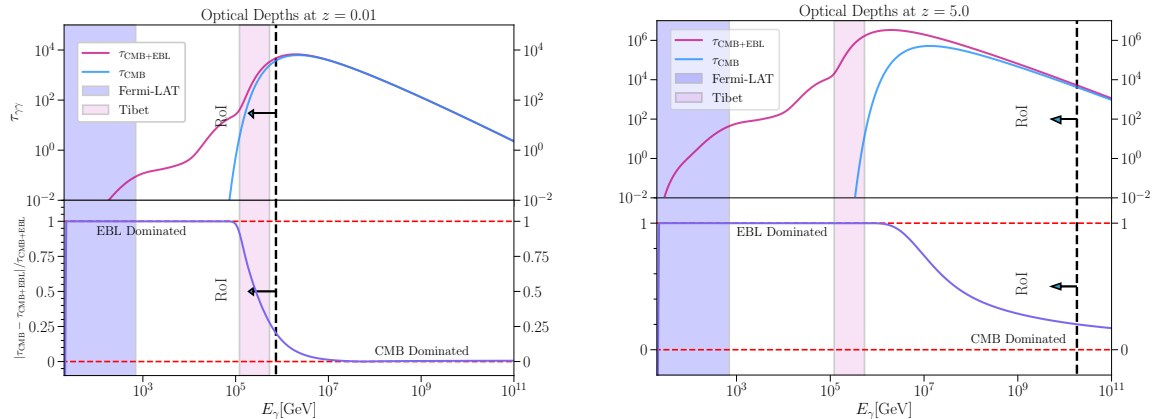


**Figure 4:** Optical depths (top panels) and their ratios (bottom panels) for a source of fixed distance within the galactic scale (left) and on the extragalactic scale (right). In the top panels, the purple (blue) lines corresponds to a target background consisting of the CMB with (without) the EBL contribution for Dominguez *et al.* model [55]. The bottom panels shows the magnitude by which the CMB-only optical depth deviates from the CMB+EBL optical depth, illustrating the energy ranges where the EBL is significant in determining the absorption of gamma-rays as they travel to Earth. The dashed vertical line indicates the region that we define to be “EBL Dominated”, or where the quantity plotted on the bottom panel is greater than 0.3. We call this as the “Region of Interest” (RoI), and it demarcates the transition between the region where the EBL is dominant according to our calculation and the region where the CMB becomes the dominant target background.

For photons of energy  $E_\gamma$  emitted by a source at a redshift  $z$ , this is given by

$$\tau_{\gamma\gamma} = \int_0^z dz' \frac{c}{(1+z)H(z)} \int_0^2 d\mu \frac{\mu}{2} \int_0^\infty d\epsilon \sigma_{\gamma\gamma}(E_\gamma, \epsilon) n_\gamma(\epsilon, z'), \quad \mu = 1 - \cos\theta, \quad (3.1)$$

where the final integral is over all possible target photon energies  $\epsilon$ ,  $\sigma_{\gamma\gamma}$  is the pair-production cross-section [46], and  $n_\gamma$  is the differential number density of photons in the target background, *i.e.*  $n = n_{\text{CMB}} + n_{\text{EBL}}$ . When the target background is the CMB, the number density at redshift  $z = 0$  is given by a Planck distribution, namely

$$n_{\text{CMB}}(\epsilon) = \frac{\epsilon^2}{\pi^2} \frac{1}{e^{\epsilon/T_{\text{CMB}}} - 1}, \quad (3.2)$$

with  $T_{\text{CMB}} = 2.348 \times 10^{-4}$  eV. In Fig. 3, we show the gamma-ray opacity as a function of gamma-ray energy for different distances and redshifts with and without the EBL contribution according to the model by Dominguez *et al.*. At energies of around  $\sim 1$  PeV, the CMB dominates the development of electromagnetic cascades, whereas the EBL starts to become relevant at lower energies. The EBL contribution relative to the CMB, in particular, also becomes more significant with increasing distances of the emission regions of the primary gamma-rays and electrons. As can be seen in Fig. 3 (right), which displays opacities at the extragalactic scale, the EBL contribution becomes considerably dominant at redshifts larger than  $z = 0.01$ ; however, its effects can already be seen at the galactic scale as shown in Fig. 3 (left).

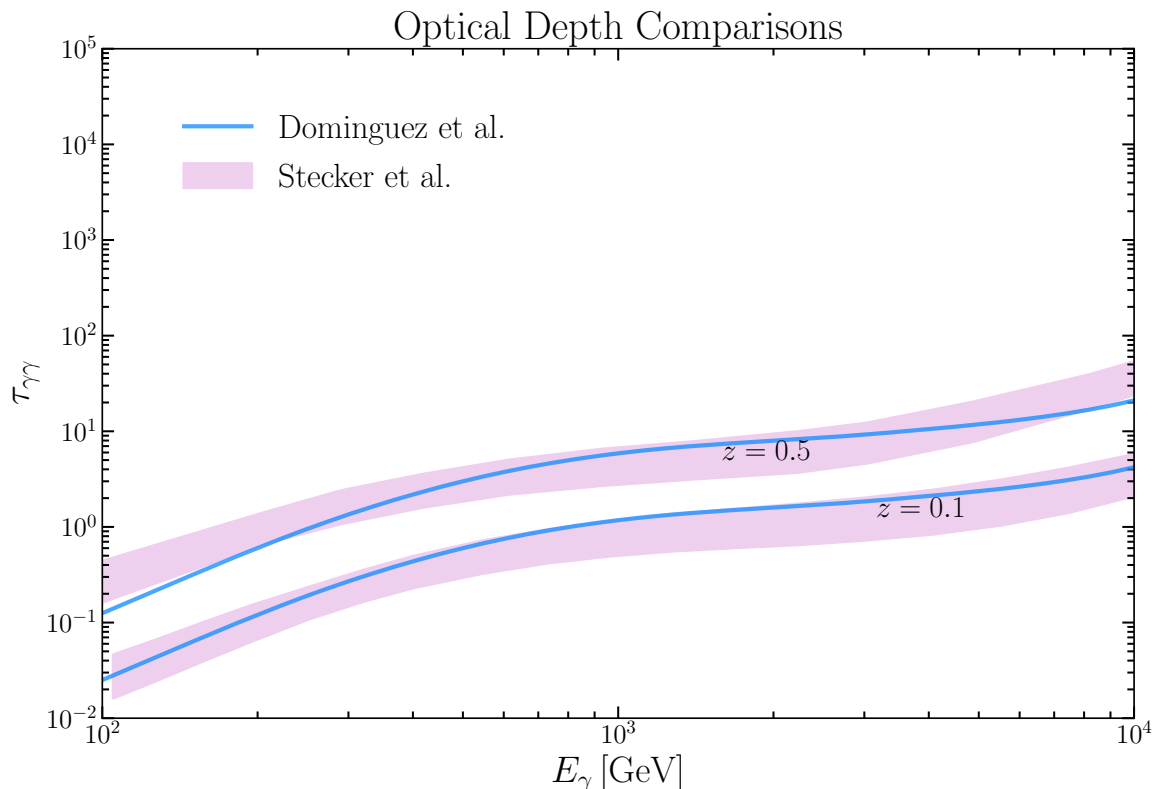


**Figure 5:** Optical depths at various redshifts as predicted by the Dominguez *et al.* [55] and Stecker *et al.* [56] EBL models. The purple band spans the range between the Stecker *et al.* Minimal and Maximal models.

The relative contributions of the EBL can also be seen in Fig. 4, where we show the optical depths for sources at two fixed distances. The bottom panels of this figure illustrate the portion of the combined optical depth ( $\tau_{\text{CMB+EBL}}$ ) that is due to interactions with the EBL, indicating the energy ranges where the EBL is relevant, denoted by an arrow as the Region of Interest (RoI). At both of the redshifts that we consider, the EBL becomes important in the energy ranges spanned by both Fermi-LAT and Tibet experiments, suggesting that any differences in the EBL could have implications for dark matter decay limits obtained using these datasets. Additionally, Fig. 5 shows the optical depths that the two EBL models we consider predict for a range of redshifts and gamma-ray beam energies. Across these ranges, the opacity exhibits differences among these models.

## 4 Analysis and Results

The motivation behind this work is to address the previously-obtained gamma-ray dark matter constraints that disfavor the decaying dark matter hypothesis for IceCube neutrino observations and to examine the effects that the uncertainty of the EBL has on those constraints and whether this implicates previous conclusions about dark matter. Hereafter, we obtain dark matter limits for the  $b\bar{b}$  decay channel with the latest high-energy neutrino and gamma-ray data and compare our results with previous limits to illustrate the EBL effect. We focus on the 7.5-year HESE sample, which has access to the prompt dark matter neutrino flux

from the whole sky (and in particular from the Galactic center), thus providing the dominant constraints on the large-mass range. Regarding gamma-rays, we analyze the data collected by Tibet AS $_{\gamma}$  and Fermi-LAT experiments. The former has observed for the first time the Galactic emission in the sub-PeV range and is therefore sensitive primarily to the dark matter galactic component. On the other hand, the latter constrains the dark matter extragalactic component by measuring the IGRB over energies lower than a few TeV. To derive lower limits on the dark matter lifetime  $\tau_{\text{DM}}$ , for each of the three experiments we consider the following likelihood in the spirit of [88]:

$$\mathcal{L}_{\text{exp}}(\tau_{\text{DM}}, m_{\text{DM}}) = \prod_i^{n_{\text{bins}}} \begin{cases} \mathcal{P}(\phi_i^{\text{exp}}(E_i) | \phi_i^{\text{DM}}(E_i)) & (\phi_i^{\text{exp}}(E_i) < \phi_i^{\text{DM}}(E_i)) \\ 1 & (\phi_i^{\text{exp}}(E_i) \geq \phi_i^{\text{DM}}(E_i)) \end{cases}, \quad (4.1)$$

where  $\phi_i^{\text{DM}}(E_i; \tau_{\text{DM}}, m_{\text{DM}})$  is the predicted energy-integrated flux on the  $i$ -th data bin,  $\phi_i^{\text{exp}}(E_i)$  the measured value by the experiment, and  $\mathcal{P}$  is a Gaussian likelihood. The width of this distribution is given by the sum of the squares of the errors, which consist of statistical errors from our Monte Carlo generation and experimental errors from the data. We then place a constraint on  $\tau_{\text{DM}}$  for a given  $m_{\text{DM}}$  assuming Wilks' theorem with one degree of freedom.

The Tibet AS $_{\gamma}$  likelihood analysis is carried out by comparing our galactic gamma-ray dark matter distributions to the data obtained in the angular window  $|b| < 5^{\circ}$  and  $25^{\circ} < l < 100^{\circ}$  in the three energy bins roughly defined by [100 TeV, 160 TeV], [160 TeV, 400 TeV], and [400 TeV, 1 PeV] [64]. In particular, we calculate the likelihood for five different dark matter masses ranging from 1 PeV to 10 PeV, since for smaller masses the dark matter contribution to Tibet AS $_{\gamma}$  data is almost negligible. Figure 6 shows an example of the final result obtained from the combination of simulation and subsequent reweighting for  $m_{\text{DM}} = 1$  PeV and  $\tau_{\text{DM}} = 10^{27}$  s, using the Stecker *et al.* Minimal model (dashed purple line) and the Dominguez *et al.* model (solid cyan line). As expected, the dominant contribution to the change in the final dark matter spectrum is an overall attenuation factor caused by gamma-ray absorption. As a result of the short propagation distances, secondary gamma-rays and the inverse-Compton process are merely subleading effects, thus implying a very small uncertainty due to the choice for the EBL model. Hence, the contributions to the  $\Delta\chi^2 = -2 \ln \mathcal{L}_{\text{exp}}$  (shown in the lower panel in Fig. 6), and consequently the lower limits on  $\tau_{\text{DM}}$ , are essentially the same for the different EBL models considered. This remains true across all the dark matter masses that we consider in this work.

For Fermi-LAT likelihood analysis, we use the P7REP IGRB HI sample, whose data are given as raw energy and positions in the sky [65]. Here, we ignore the spatial distribution and bin the data into 40 energy bins, equally spaced in logarithmic space from 200 MeV to 2 TeV. The Fermi-LAT likelihood is then calculated for eleven different dark matter masses ranging from  $10^{5.25}$  GeV to 10 PeV. As can be seen in Fig. 1, where we show an example of the final result obtained from the simulation and subsequent reweighting for a dark matter mass of 1 PeV decaying to  $b\bar{b}$ , there is a visibly significant production of secondary gamma-rays as photons propagate to Earth, indicating that the dominant production mechanisms for visible gamma-rays from extragalactic sources are the  $\gamma \rightarrow \gamma$  and  $e^+e^- \rightarrow \gamma$  secondary contributions.<sup>2</sup> This results into a significant uncertainty due to the EBL models on the dark matter constraints as shown in Fig. 7. The three lines represent the lower bounds at 95% confidence level on the dark matter lifetime for the  $b\bar{b}$  decay channel obtained for

<sup>2</sup>The comparison of these two different components to data and the contributions to the  $\Delta\chi^2$  for different dark matter masses and EBL models are reported in Appendix B.

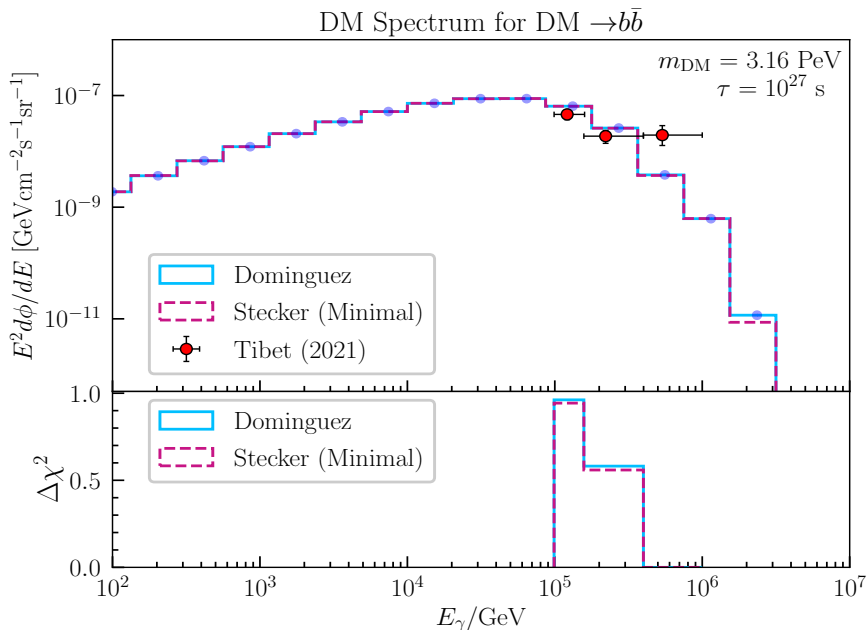


**Figure 6:** Final galactic dark matter decay spectra for a chosen dark-matter mass and a lifetime of  $10^{27}$  seconds. The two lines correspond to two different EBL models. The bottom panel shows the  $\Delta\chi^2$  calculated by comparing our Monte Carlo simulations to Tibet  $AS_\gamma$  data [64].

different EBL models: Stecker *et al.* Maximal model produces the weaker lower bound (blue line), while the Minimal one produces the strongest limit (light purple line); the model by Dominguez *et al.* lies in between (dark purple line).

Our results obtained using neutrinos and gamma-rays are shown in Fig. 8 for the galactic (left plot) and extragalactic (right plot) dark matter components, separately. In particular, the dark blue lines represent the constraints placed by IceCube data, while the light (dark) purple lines in the left (right) plot corresponds to Tibet  $AS_\gamma$  (Fermi-LAT) data. In the right plot, the purple band represents the allowed range within which the EBL models we consider give predictions for the lower limit of the dark matter lifetime. The purple dashed line within this band reflects the average taken over these EBL models. We find that the gamma-ray limits derived with the galactic data are weaker with respect to the ones from Fermi-LAT observations (for  $m_{DM}$  smaller than 10 PeV), and that in general neutrino limits are stronger than gamma-ray ones.

Along with our constrains, we also plot other neutrino and gamma-ray constraints obtained outside of this work. We emphasize that, in contrast to previously reported analyses in the literature, our analysis is background agnostic; *i.e.*, we do not consider fitting to an astrophysical component for both neutrino and gamma-ray data. However, regarding neutrino limits, we find improved constraints with respect to the works by Bhattacharya *et al.* [35] and Chianese *et al.* [36]. This is despite the fact that both of these analyses attempt to model the astrophysical background flux by means of a power-law distribution. Aside from this, however, here are several additional differences in our analyses, data collection, and likelihood treatments that could account for the overall improvement in our neutrino constraints. First, [35] uses six years of runtime with energies above 10 TeV and [36] uses the

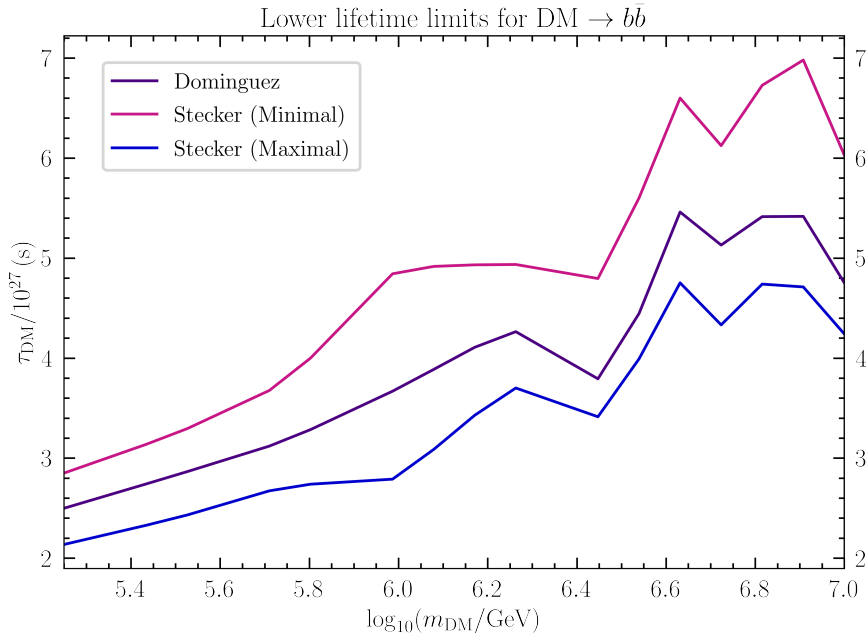


**Figure 7:** Fermi-LAT lower bounds at 95% CL obtained for the three different EBL models considered in this work.

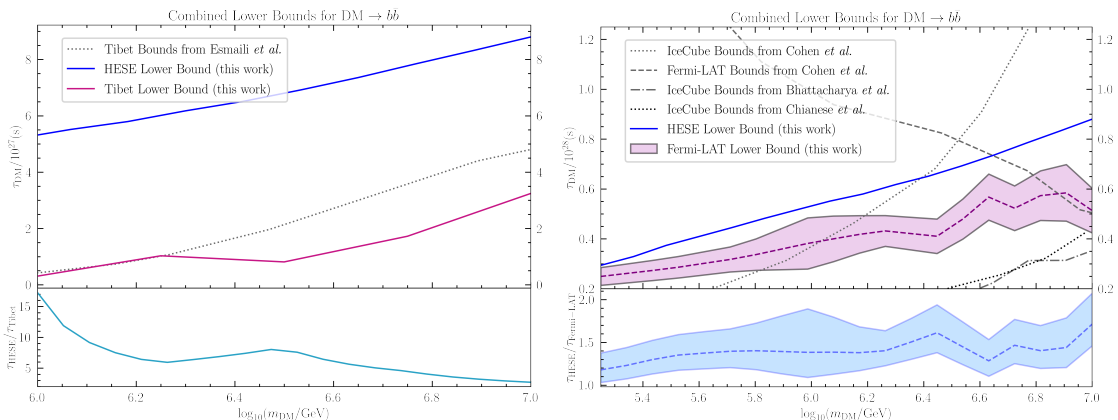


**Figure 8:** Lower limits at 95% CL on the dark matter lifetime derived from IceCube 7.5-year HESE flux data (blue lines), Tibet  $AS_\gamma$  data (light purple line) and Fermi-LAT diffuse measurements (dark purple band). The left and right plots refer to galactic and extragalactic gamma-ray data, respectively. The dark purple band represents the uncertainty due to different modeling of the EBL spectrum. The lower panels show the ration between the neutrino HESE limits and the galactic (left) and extragalactic (right) gamma-ray limits we obtain. Also shown with gray thin lines are previous bounds [35, 36, 48, 52].

preliminary 7.5 years of HESE event data, whereas our analysis uses the true 7.5 year HESE flux data. Second, for the galactic dark matter distribution we rely on a generalized NFW profile with parameters that were obtained by minimizing over the chi-squared distributions provided by the recent work [66]. Finally, to obtain the predicted dark matter fluxes, our analysis uses the recent code `HDMSpectra` which extends the calculations of the electroweak

radiative corrections to Planck-scale dark matter masses. For the  $b\bar{b}$  decay channel, these processes significantly change the energy distribution of the neutrinos produced, yielding a harder neutrino spectrum compared to the ones obtained by means of other software such as PYTHIA 8.2 [89] and PPPC [90](used in the analyses [35] and [36], respectively), which in-turn produces a stronger result.

Regarding the gamma-ray constraints, our analysis on galactic data obtains similar bounds to the ones obtained by Esmaili *et al.* [52]. On the other hand, our results based on extragalactic data differ from the analysis performed by Cohen *et al.* [48]. The latter considers peculiar regions around the Galactic center (see Fig. S4 in [48]), where the dominant contribution from decaying dark matter comes from the prompt galactic component and the secondary galactic  $e^+e^- \rightarrow \gamma$  component from Inverse-Compton scattering. We instead focus on the IGRB data from the whole sky and find that the extragalactic dark matter flux is the dominant contribution. Moreover, Cohen *et al.* model the photon background, whereas we take a model agnostic approach. By construction, our resulting constraints are weaker than those that are background informed, as can be seen in the right plot of Fig. 8, where previous constraints are significantly stronger for masses smaller than  $10^{6.5}$  GeV. However, at the largest masses, we find good agreement with [48], particularly when comparing to our mean prediction.<sup>3</sup> The width of the EBL uncertainty band allows for even stronger constraints that potentially extend to higher dark matter masses. At the highest masses that we consider, this uncertainty gives rise to deviations of up to 40% in lifetime. For  $m_{\text{DM}} = 1$  PeV, the EBL uncertainty amounts to a  $\sim 55\%$  variation for the dark matter lower bound on the lifetime.

Finally, we comment on the relative strengths of the gamma-ray and neutrino constraints obtained in this work. These are shown in the bottom panels of Fig. 8, where we plot the ratio between the lifetime neutrino constraints and the gamma-ray constraints. Since the flux is inversely proportional to the lifetime, this ratio is proportional to the ratio of the dark matter fluxes between neutrinos and photons. We find that this ratio is always greater than one in the mass range given, even when accounting for the EBL uncertainties. This implies that in a background agnostic treatment a significant fraction of the neutrino flux observed in HESE can be accommodated with a dark matter component. However, regarding the extragalactic gamma-ray limit, when the background is modeled, the constraint from Cohen *et al.* applies and then we find that this ratio is less than one below approximately  $m_{\text{DM}} = 10^{6.5}$  GeV, and greater than one for higher masses. Our results highlight the importance of properly modeling the gamma-ray background in the Fermi-LAT data to derive proper constraints and, moreover, that at the highest masses, the neutrino constraints dominate over the gamma-ray limits.

## 5 Conclusions

In this work, we present newly-obtained neutrino and gamma-ray limits on galactic and extragalactic dark matter decay. We initialize dark matter decay spectra for neutrinos, gamma-rays, electrons and positrons, and we propagate these to Earth using three different models for the EBL: Dominguez *et al.* and the Stecker *et al.* Minimal and Maximal models. We then compare our spectra to the 7.5-year IceCube HESE sample, the Tibet AS $_{\gamma}$  2021 data, and the Fermi-LAT diffuse data. The resulting background-agnostic analysis that we carry out yields constraints that are, taken by themselves, consistent with a decaying dark matter component explaining the HESE data, therefore providing some motivation for considering

<sup>3</sup>The almost flat behaviour of our limit is indeed in agreement with one placed by Cohen *et al.* for the extragalactic dark matter component only (see Fig. S13 in [48]).

this as a partial explanation for the tension between the HESE analysis and the Northern tracks data analysis regarding the nature of the astrophysical neutrino spectrum. Figure 8 summarizes our results, showing that the lower bounds estimated for decaying heavy dark matter can vary by up to  $\sim 55\%$  (for 1 PeV) and up to  $\sim 40\%$  at the larger mass end, due to the current uncertainty on the EBL spectrum. In comparison to previously-obtained limits using gamma-rays and neutrinos, our constraints are in some respects better, but in other respects they can be made more robust by incorporating a background model.

Our work motivates performing a similar investigation of the effects of the EBL on multi-messenger signals from other kinds of astrophysical sources. Finally, modeling a gamma-ray and neutrino background is an important step in determining the extent to which high-energy neutrinos observed in samples such as HESE or the through-going muon tracks come from heavy dark matter decay. However, this astrophysical background comes from as yet unidentified sources.

## Acknowledgments

We thank Aaron C. Vincent and Sergio Palomares-Ruiz for useful comments and discussions, and Rafael Alves Batista for clarifications about CRPropa. CAA and BS are supported by the Faculty of Arts and Sciences of Harvard University. Additionally, CAA thanks the Alfred P. Sloan Foundation for their support. MC is supported by the research grant number 2017W4HA7S “NAT-NET: Neutrino and Astroparticle Theory Network” under the program PRIN 2017 funded by the Italian Ministero dell’Università e della Ricerca (MUR) and by the research project TASP (Theoretical Astroparticle Physics) funded by the Istituto Nazionale di Fisica Nucleare (INFN).

## References

- [1] M. Ackermann et al., *Astrophysics Uniquely Enabled by Observations of High-Energy Cosmic Neutrinos*, *Bull. Am. Astron. Soc.* **51** (2019) 185 [[1903.04334](#)].
- [2] M. Ackermann et al., *Fundamental Physics with High-Energy Cosmic Neutrinos*, *Bull. Am. Astron. Soc.* **51** (2019) 215 [[1903.04333](#)].
- [3] M. Ackermann et al., *High-Energy and Ultra-High-Energy Neutrinos*, [2203.08096](#).
- [4] P. Mészáros, D.B. Fox, C. Hanna and K. Murase, *Multi-Messenger Astrophysics*, *Nature Rev. Phys.* **1** (2019) 585 [[1906.10212](#)].
- [5] R. Alves Batista et al., *EuCAPT White Paper: Opportunities and Challenges for Theoretical Astroparticle Physics in the Next Decade*, [2110.10074](#).
- [6] ICECUBE collaboration, *The IceCube high-energy starting event sample: Description and flux characterization with 7.5 years of data*, *Phys. Rev. D* **104** (2021) 022002 [[2011.03545](#)].
- [7] A. Loeb and E. Waxman, *The Cumulative background of high energy neutrinos from starburst galaxies*, *JCAP* **05** (2006) 003 [[astro-ph/0601695](#)].
- [8] A. Ambrosone, M. Chianese, D.F.G. Fiorillo, A. Marinelli, G. Miele and O. Pisanti, *Starburst galaxies strike back: a multi-messenger analysis with Fermi-LAT and IceCube data*, *Mon. Not. Roy. Astron. Soc.* **503** (2021) 4032 [[2011.02483](#)].
- [9] W. Winter, *Photohadronic Origin of the TeV-PeV Neutrinos Observed in IceCube*, *Phys. Rev. D* **88** (2013) 083007 [[1307.2793](#)].
- [10] D.F.G. Fiorillo, A. Van Vliet, S. Morisi and W. Winter, *Unified thermal model for photohadronic neutrino production in astrophysical sources*, *JCAP* **07** (2021) 028 [[2103.16577](#)].

- [11] MAGIC collaboration, *The blazar TXS 0506+056 associated with a high-energy neutrino: insights into extragalactic jets and cosmic ray acceleration*, *Astrophys. J. Lett.* **863** (2018) L10 [[1807.04300](#)].
- [12] ICECUBE, FERMI-LAT, MAGIC, AGILE, ASAS-SN, HAWC, H.E.S.S., INTEGRAL, KANATA, KISO, KAPTEYN, LIVERPOOL TELESCOPE, SUBARU, SWIFT NUSTAR, VERITAS, VLA/17B-403 collaboration, *Multimessenger observations of a flaring blazar coincident with high-energy neutrino IceCube-170922A*, *Science* **361** (2018) eaat1378 [[1807.08816](#)].
- [13] ICECUBE collaboration, *Neutrino emission from the direction of the blazar TXS 0506+056 prior to the IceCube-170922A alert*, *Science* **361** (2018) 147 [[1807.08794](#)].
- [14] ICECUBE collaboration, *Improved Characterization of the Astrophysical Muon-Neutrino Flux with 9.5 Years of IceCube Data*, [2111.10299](#).
- [15] E. Waxman and J. Bahcall, *High energy neutrinos from astrophysical sources: An upper bound*, *Physical Review D* **59** (1998) .
- [16] C.-Y. Chen, P.S. Bhupal Dev and A. Soni, *Two-component flux explanation for the high energy neutrino events at IceCube*, *Phys. Rev. D* **92** (2015) 073001 [[1411.5658](#)].
- [17] ICECUBE collaboration, *A combined maximum-likelihood analysis of the high-energy astrophysical neutrino flux measured with IceCube*, *Astrophys. J.* **809** (2015) 98 [[1507.03991](#)].
- [18] D. Gaggero, D. Grasso, A. Marinelli, A. Urbano and M. Valli, *The gamma-ray and neutrino sky: A consistent picture of Fermi-LAT, Milagro, and IceCube results*, *Astrophys. J. Lett.* **815** (2015) L25 [[1504.00227](#)].
- [19] M. Chianese, G. Miele, S. Morisi and E. Vitagliano, *Low energy IceCube data and a possible Dark Matter related excess*, *Phys. Lett. B* **757** (2016) 251 [[1601.02934](#)].
- [20] A. Palladino and F. Vissani, *Extragalactic plus Galactic model for IceCube neutrino events*, *Astrophys. J.* **826** (2016) 185 [[1601.06678](#)].
- [21] A.C. Vincent, S. Palomares-Ruiz and O. Mena, *Analysis of the 4-year IceCube high-energy starting events*, *Phys. Rev. D* **94** (2016) 023009 [[1605.01556](#)].
- [22] A. Palladino, M. Spurio and F. Vissani, *On the IceCube spectral anomaly*, *JCAP* **12** (2016) 045 [[1610.07015](#)].
- [23] L.A. Anchordoqui, M.M. Block, L. Durand, P. Ha, J.F. Soriano and T.J. Weiler, *Evidence for a break in the spectrum of astrophysical neutrinos*, *Phys. Rev. D* **95** (2017) 083009 [[1611.07905](#)].
- [24] P.B. Denton, D. Marfatia and T.J. Weiler, *The Galactic Contribution to IceCube's Astrophysical Neutrino Flux*, *JCAP* **08** (2017) 033 [[1703.09721](#)].
- [25] M. Chianese, R. Mele, G. Miele, P. Migliozzi and S. Morisi, *Use of ANTARES and IceCube Data to Constrain a Single Power-law Neutrino Flux*, *Astrophys. J.* **851** (2017) 36 [[1707.05168](#)].
- [26] A. Palladino and W. Winter, *A multi-component model for observed astrophysical neutrinos*, *Astron. Astrophys.* **615** (2018) A168 [[1801.07277](#)].
- [27] Y. Sui and P.S. Bhupal Dev, *A Combined Astrophysical and Dark Matter Interpretation of the IceCube HESE and Throughgoing Muon Events*, *JCAP* **07** (2018) 020 [[1804.04919](#)].
- [28] B. Feldstein, A. Kusenko, S. Matsumoto and T.T. Yanagida, *Neutrinos at IceCube from Heavy Decaying Dark Matter*, *Phys. Rev. D* **88** (2013) 015004 [[1303.7320](#)].
- [29] A. Esmaili and P.D. Serpico, *Are IceCube neutrinos unveiling PeV-scale decaying dark matter?*, *JCAP* **11** (2013) 054 [[1308.1105](#)].
- [30] Y. Bai, R. Lu and J. Salvado, *Geometric Compatibility of IceCube TeV-PeV Neutrino Excess and its Galactic Dark Matter Origin*, *JHEP* **01** (2016) 161 [[1311.5864](#)].

- [31] A. Bhattacharya, M.H. Reno and I. Sarcevic, *Reconciling neutrino flux from heavy dark matter decay and recent events at IceCube*, *JHEP* **06** (2014) 110 [[1403.1862](#)].
- [32] A. Esmaili, S.K. Kang and P.D. Serpico, *IceCube events and decaying dark matter: hints and constraints*, *JCAP* **12** (2014) 054 [[1410.5979](#)].
- [33] M. Kachelriess, O.E. Kalashev and M.Y. Kuznetsov, *Heavy decaying dark matter and IceCube high energy neutrinos*, *Phys. Rev. D* **98** (2018) 083016 [[1805.04500](#)].
- [34] P.B. Denton and I. Tamborra, *Invisible Neutrino Decay Could Resolve IceCube’s Track and Cascade Tension*, *Phys. Rev. Lett.* **121** (2018) 121802 [[1805.05950](#)].
- [35] A. Bhattacharya, A. Esmaili, S. Palomares-Ruiz and I. Sarcevic, *Update on decaying and annihilating heavy dark matter with the 6-year IceCube HESE data*, *JCAP* **05** (2019) 051 [[1903.12623](#)].
- [36] M. Chianese, D.F.G. Fiorillo, G. Miele, S. Morisi and O. Pisanti, *Decaying dark matter at IceCube and its signature on High Energy gamma experiments*, *JCAP* **11** (2019) 046 [[1907.11222](#)].
- [37] A. Dekker, M. Chianese and S. Ando, *Probing dark matter signals in neutrino telescopes through angular power spectrum*, *JCAP* **09** (2020) 007 [[1910.12917](#)].
- [38] ICECUBE collaboration, *Search for neutrinos from decaying dark matter with IceCube*, *Eur. Phys. J. C* **78** (2018) 831 [[1804.03848](#)].
- [39] ICECUBE collaboration, *Searches for Connections Between Dark Matter and Neutrinos with the IceCube High-Energy Starting Event Sample*, *PoS ICRC2019* (2020) 839 [[1907.11193](#)].
- [40] ICECUBE collaboration, *A Search for Neutrinos from Decaying Dark Matter in Galaxy Clusters and Galaxies with IceCube*, *PoS ICRC2021* (2021) 506 [[2107.11527](#)].
- [41] P. Ciafaloni, D. Comelli, A. Riotto, F. Sala, A. Strumia and A. Urbano, *Weak Corrections are Relevant for Dark Matter Indirect Detection*, *JCAP* **03** (2011) 019 [[1009.0224](#)].
- [42] J. Buch, M. Cirelli, G. Giesen and M. Taoso, *PPPC 4 DM secondary: A Poor Particle Physicist Cookbook for secondary radiation from Dark Matter*, *JCAP* **09** (2015) 037 [[1505.01049](#)].
- [43] C.W. Bauer, N.L. Rodd and B.R. Webber, *Dark matter spectra from the electroweak to the Planck scale*, *JHEP* **06** (2021) 121 [[2007.15001](#)].
- [44] K. Murase and J.F. Beacom, *Constraining Very Heavy Dark Matter Using Diffuse Backgrounds of Neutrinos and Cascaded Gamma Rays*, *JCAP* **10** (2012) 043 [[1206.2595](#)].
- [45] K. Murase, R. Laha, S. Ando and M. Ahlers, *Testing the Dark Matter Scenario for PeV Neutrinos Observed in IceCube*, *Phys. Rev. Lett.* **115** (2015) 071301 [[1503.04663](#)].
- [46] A. Esmaili and P.D. Serpico, *Gamma-ray bounds from EAS detectors and heavy decaying dark matter constraints*, *JCAP* **10** (2015) 014 [[1505.06486](#)].
- [47] O.K. Kalashev and M.Y. Kuznetsov, *Constraining heavy decaying dark matter with the high energy gamma-ray limits*, *Phys. Rev. D* **94** (2016) 063535 [[1606.07354](#)].
- [48] T. Cohen, K. Murase, N.L. Rodd, B.R. Safdi and Y. Soreq,  *$\gamma$ -ray Constraints on Decaying Dark Matter and Implications for IceCube*, *Phys. Rev. Lett.* **119** (2017) 021102 [[1612.05638](#)].
- [49] HAWC collaboration, *A Search for Dark Matter in the Galactic Halo with HAWC*, *JCAP* **02** (2018) 049 [[1710.10288](#)].
- [50] C. Blanco and D. Hooper, *Constraints on Decaying Dark Matter from the Isotropic Gamma-Ray Background*, *JCAP* **03** (2019) 019 [[1811.05988](#)].
- [51] K. Ishiwata, O. Macias, S. Ando and M. Arimoto, *Probing heavy dark matter decays with multi-messenger astrophysical data*, *JCAP* **01** (2020) 003 [[1907.11671](#)].

- [52] A. Esmaili and P.D. Serpico, *First implications of Tibet AS $\gamma$  data for heavy dark matter*, *Phys. Rev. D* **104** (2021) L021301 [[2105.01826](#)].
- [53] T.N. Maity, A.K. Saha, A. Dubey and R. Laha, *Search for dark matter using sub-PeV  $\gamma$ -rays observed by Tibet AS $\gamma$* , *Phys. Rev. D* **105** (2022) L041301 [[2105.05680](#)].
- [54] M. Chianese, D.F.G. Fiorillo, R. Hajjar, G. Miele and N. Saviano, *Constraints on heavy decaying dark matter with current gamma-ray measurements*, *JCAP* **11** (2021) 035 [[2108.01678](#)].
- [55] A. Dominguez et al., *Extragalactic Background Light Inferred from AEGIS Galaxy SED-type Fractions*, *Mon. Not. Roy. Astron. Soc.* **410** (2011) 2556 [[1007.1459](#)].
- [56] F.W. Stecker, S.T. Scully and M.A. Malkan, *An Empirical Determination of the Intergalactic Background Light from UV to FIR Wavelengths Using FIR Deep Galaxy Surveys and the Gamma-ray Opacity of the Universe*, *Astrophys. J.* **827** (2016) 6 [[1605.01382](#)].
- [57] J.D. Finke, S. Razzaque and C.D. Dermer, *Modeling the Extragalactic Background Light from Stars and Dust*, *Astrophys. J.* **712** (2010) 238 [[0905.1115](#)].
- [58] T.M. Kneiske and H. Dole, *A Lower-Limit Flux for the Extragalactic Background Light*, *Astron. Astrophys.* **515** (2010) A19 [[1001.2132](#)].
- [59] R.C. Gilmore, R.S. Somerville, J.R. Primack and A. Domínguez, *Semi-analytic modelling of the extragalactic background light and consequences for extragalactic gamma-ray spectra*, *Monthly Notices of the RAS* **422** (2012) 3189 [[1104.0671](#)].
- [60] K. Helgason and A. Kashlinsky, *Reconstructing the  $\gamma$ -ray Photon Optical Depth of the Universe to  $z \sim 4$  from Multiwavelength Galaxy Survey Data*, *Astrophys. J. Lett.* **758** (2012) L13 [[1208.4364](#)].
- [61] Y. Inoue, S. Inoue, M.A.R. Kobayashi, R. Makiya, Y. Niino and T. Totani, *Extragalactic Background Light from Hierarchical Galaxy Formation: Gamma-ray Attenuation up to the Epoch of Cosmic Reionization and the First Stars*, *Astrophys. J.* **768** (2013) 197 [[1212.1683](#)].
- [62] A. Franceschini and G. Rodighiero, *The extragalactic background light revisited and the cosmic photon-photon opacity*, *Astronomy and Astrophysics* **603** (2017) A34 [[1705.10256](#)].
- [63] S.K. Andrews, S.P. Driver, L.J. Davies, C.d.P. Lagos and A.S.G. Robotham, *Modelling the cosmic spectral energy distribution and extragalactic background light over all time*, *Mon. Not. Roy. Astron. Soc.* **474** (2018) 898 [[1710.11329](#)].
- [64] TIBET ASGAMMA collaboration, *First Detection of sub-PeV Diffuse Gamma Rays from the Galactic Disk: Evidence for Ubiquitous Galactic Cosmic Rays beyond PeV Energies*, *Phys. Rev. Lett.* **126** (2021) 141101 [[2104.05181](#)].
- [65] FERMI-LAT collaboration, *The spectrum of isotropic diffuse gamma-ray emission between 100 MeV and 820 GeV*, *Astrophys. J.* **799** (2015) 86 [[1410.3696](#)].
- [66] M. Benito, F. Iocco and A. Cuoco, *Uncertainties in the galactic dark matter distribution: An update*, *Physics of the Dark Universe* **32** (2021) 100826.
- [67] PLANCK collaboration, *Planck 2018 results. VI. Cosmological parameters*, *Astron. Astrophys.* **641** (2020) A6 [[1807.06209](#)].
- [68] V.S. Berezinsky and A.Y. Smirnov, *Cosmic neutrinos of ultra-high energies and detection possibility*, *Astrophys. Space Sci.* **32** (1975) 461.
- [69] P.S. Coppi and F.A. Aharonian, *Constraints on the VHE emissivity of the universe from the diffuse GeV gamma-ray background*, *Astrophys. J. Lett.* **487** (1997) L9 [[astro-ph/9610176](#)].
- [70] T.M. Venters, *Contribution to the Extragalactic Gamma-ray Background from the Cascades of Very-high Energy Gamma Rays from Blazars*, *Astrophys. J.* **710** (2010) 1530 [[1001.1363](#)].

- [71] K. Murase, J.F. Beacom and H. Takami, *Gamma-Ray and Neutrino Backgrounds as Probes of the High-Energy Universe: Hints of Cascades, General Constraints, and Implications for TeV Searches*, *JCAP* **08** (2012) 030 [[1205.5755](#)].
- [72] V. Berezhinsky and O. Kalashev, *High energy electromagnetic cascades in extragalactic space: physics and features*, *Phys. Rev. D* **94** (2016) 023007 [[1603.03989](#)].
- [73] S. Lee, *Propagation of extragalactic high energy cosmic and  $\gamma$  rays*, *Phys. Rev. D* **58** (1998) 043004.
- [74] A.E. Vladimirov, S.W. Digel, G. Johannesson, P.F. Michelson, I.V. Moskalenko, P.L. Nolan et al., *GALPROP WebRun: an internet-based service for calculating galactic cosmic ray propagation and associated photon emissions*, *Comput. Phys. Commun.* **182** (2011) 1156 [[1008.3642](#)].
- [75] M. Kachelriess, S. Ostapchenko and R. Tomas, *ELMAG: A Monte Carlo simulation of electromagnetic cascades on the extragalactic background light and in magnetic fields*, *Comput. Phys. Commun.* **183** (2012) 1036 [[1106.5508](#)].
- [76] O.E. Kalashev and E. Kido, *Simulations of Ultra High Energy Cosmic Rays propagation*, *J. Exp. Theor. Phys.* **120** (2015) 790 [[1406.0735](#)].
- [77] C. Blanco,  *$\gamma$ -cascade: a simple program to compute cosmological gamma-ray propagation*, *JCAP* **01** (2019) 013 [[1804.00005](#)].
- [78] R. Alves Batista, A. Dundovic, M. Erdmann, K.-H. Kampert, D. Kuempel, G. Müller et al., *CRPropa 3 - a Public Astrophysical Simulation Framework for Propagating Extraterrestrial Ultra-High Energy Particles*, *JCAP* **05** (2016) 038 [[1603.07142](#)].
- [79] C. Heiter, D. Kuempel, D. Walz and M. Erdmann, *Production and propagation of ultra-high energy photons using CRPropa 3*, *Astropart. Phys.* **102** (2018) 39 [[1710.11406](#)].
- [80] S.P. Driver, S.K. Andrews, L.J. Davies, A.S.G. Robotham, A.H. Wright, R.A. Windhorst et al., *Measurements of Extragalactic Background Light From the far UV to the far IR From Deep Ground- and Space-based Galaxy Counts*, *Astrophys. J.* **827** (2016) 108 [[1605.01523](#)].
- [81] FERMI-LAT collaboration, *A gamma-ray determination of the Universe's star formation history*, *Science* **362** (2018) 1031 [[1812.01031](#)].
- [82] K.K. Singh and P.J. Meintjes, *Extragalactic background light models and GeV-TeV observation of blazars*, [2004.01933](#).
- [83] A. Saveliev and R. Alves Batista, *The intrinsic gamma-ray spectrum of TXS 0506+056: intergalactic propagation effects*, *Mon. Not. Roy. Astron. Soc.* **500** (2020) 2188 [[2009.09772](#)].
- [84] E. Dwek and F. Krennrich, *The extragalactic background light and the gamma-ray opacity of the universe*, *Astroparticle Physics* **43** (2013) 112.
- [85] J. Biteau and D.A. Williams, *THE EXTRAGALACTIC BACKGROUND LIGHT, THE HUBBLE CONSTANT, AND ANOMALIES: CONCLUSIONS FROM 20 YEARS OF TeV GAMMA-RAY OBSERVATIONS*, *The Astrophysical Journal* **812** (2015) 60.
- [86] A.U. Abeysekara, A. Archer, W. Benbow, R. Bird, A. Brill, R. Brose et al., *Measurement of the extragalactic background light spectral energy distribution with VERITAS*, *The Astrophysical Journal* **885** (2019) 150.
- [87] and H. Abdalla, A. Abramowski, F. Aharonian, F.A. Benkhali, A.G. Akhperjanian, T. Andersson et al., *Measurement of the EBL spectral energy distribution using the VHE  $\gamma$ -ray spectra of h.e.s.s. blazars*, *Astronomy Astrophysics* **606** (2017) A59.
- [88] C.A. Argüelles, A. Diaz, A. Kheirandish, A. Olivares-Del-Campo, I. Safa and A.C. Vincent, *Dark matter annihilation to neutrinos*, *Rev. Mod. Phys.* **93** (2021) 035007 [[1912.09486](#)].

- [89] T. Sjöstrand, S. Ask, J.R. Christiansen, R. Corke, N. Desai, P. Ilten et al., *An introduction to PYTHIA 8.2*, *Comput. Phys. Commun.* **191** (2015) 159 [[1410.3012](#)].
- [90] M. Cirelli, G. Corcella, A. Hektor, G. Hutsi, M. Kadastik, P. Panci et al., *PPPC 4 DM ID: A Poor Particle Physicist Cookbook for Dark Matter Indirect Detection*, *JCAP* **03** (2011) 051 [[1012.4515](#)].
- [91] R. Jansson and G.R. Farrar, *A NEW MODEL OF THE GALACTIC MAGNETIC FIELD*, *The Astrophysical Journal* **757** (2012) 14.

## A Simulation Details

To propagate photons, electrons, and positrons over galactic and extragalactic scales, we use `CRPropa` [78], a tool developed to simulate ultra-high-energy nuclei within galactic and extragalactic environments. For the propagations that we simulate in `CRPropa`, we enable the following processes: pair production, double pair production, triplet pair production, Inverse-Compton scattering, and synchrotron radiation. For galactic propagation, we set the magnetic field to be the JF12 field model [91], while for extragalactic propagation we assume no additional magnetic field contribution. In both cases, we inject an initial power-law spectrum that follows  $\phi \sim (E/E_c)^{-1}$  and which we define uniformly over a solid sphere. For the galactic case, propagation takes place over distances of 0 to 100 kpc, while for the extragalactic case, we propagate between 100 kpc and 10 Gpc. `CRPropa` creates this initial spectrum via Monte Carlo generation, where we set the number of Monte Carlo simulations to be roughly  $1.5 \times 10^6$  per injected dark matter mass. Regarding the injected spectrum, the minimum and maximum ( $E_c$ ) energies vary with the dark matter mass that we consider such that  $E_c = m_{\text{DM}}/2$  and  $E_{\text{min}} = (m_{\text{DM}}/2) \times 10^{-6}$ .

To then obtain the expected dark-matter decay spectrum from the `CRPropa` output following propagation, we apply a reweighting procedure where we group the photons that arrive at Earth according to their corresponding, unique Monte Carlo generated events. The reweighting scheme then assigns a new weight to each of these events that depends on that event's initial energy and position, such that the new weights correspond to a dark matter distribution. Schematically, the end result of this is that the our reweighting scheme takes the initial power-law distribution that is fed into `CRPropa` and returns the expected final, propagated spectrum that results from dark-matter decay for a given dark matter mass, lifetime, and decay channel. Although we apply this to the case of dark matter decay, this procedure could be generalized for any arbitrary, well-behaved distribution that needs to be propagated over some distance.

The weight that we assign to each event can be decomposed into a position weight, and energy weight, and a multiplicative prefactor that depends on dark matter parameters and that converts the result into units of flux.

### A.1 Position Reweighting

The position reweighting that we apply to each Monte Carlo event assigns a multiplicative factor replaces the Monte Carlo generation weights for a uniformly distributed source with those corresponding to the desired dark matter profile. Schematically, these position weights can be expressed as

$$w_r = \frac{w_{\text{physical}}}{w_{\text{generated}}} = \left( \rho_{\text{DM}}(r) \right) \left( \frac{D(r)}{\int_{r_{\text{min}}}^{r_{\text{max}}} D(r)} \right)^{-1} = \rho_{\text{DM}}(r)(r_{\text{max}} - r_{\text{min}}), \quad (\text{A.1})$$

where  $D(r)$  is the initial distribution,  $\rho_{\text{DM}}(r)$  is the dark matter distribution, and the denominator of the quantity in parentheses corresponds to an overall normalization included in the generated weights, which is a uniform distribution for our simulations. The physical position weights depend on the profile that we consider. For galactic reweighting, for example, we use the generalized NFW profile  $\rho_{\text{DM}}(r)$  defined in Eq. (2.2). For the extragalactic position reweighting, we use  $\rho_{\text{cr}}\Omega_{\text{DM}}/H(z)$ , where we set the parameters to the values mentioned in Section 2.

## A.2 Energy Reweighting

In a similar way, the energy reweighting acts as a multiplicative factor that replaces the Monte Carlo simulation weights for the power-law spectrum  $\phi(E) \sim E^{-1}$  generated by `CRPropa` and returns a physical weight for each event that corresponds to the dark matter decay spectrum  $\phi_{\text{DM}} \propto dN/dE$  computed by `HDMSpectra`. These energy weights can be expressed as

$$w_E = \frac{w_{\text{physical}}}{w_{\text{generated}}} = \left( \phi_{\text{DM}}(E) \right) \left( \frac{\phi(E)}{\int_{E_{\text{min}}}^{E_{\text{max}}} \phi(E)} \right)^{-1} = \phi_{\text{DM}}(E) (E \times \ln(E_{\text{max}}/E_{\text{min}})). \quad (\text{A.2})$$

For the extragalactic energy reweighting, there is also a redshift in the energy of the initial spectrum which resulting in an additional factor of  $(1+z)$ .

## B Spectra of Photons Arriving at Earth

The different IGRB predictions of the gamma-ray flux for the three EBL models and for different DM masses can be seen in Fig. 9 for the  $\gamma \rightarrow \gamma$  extragalactic secondary component, and in Fig. 10 for the  $e^+e^- \rightarrow \gamma$  one.

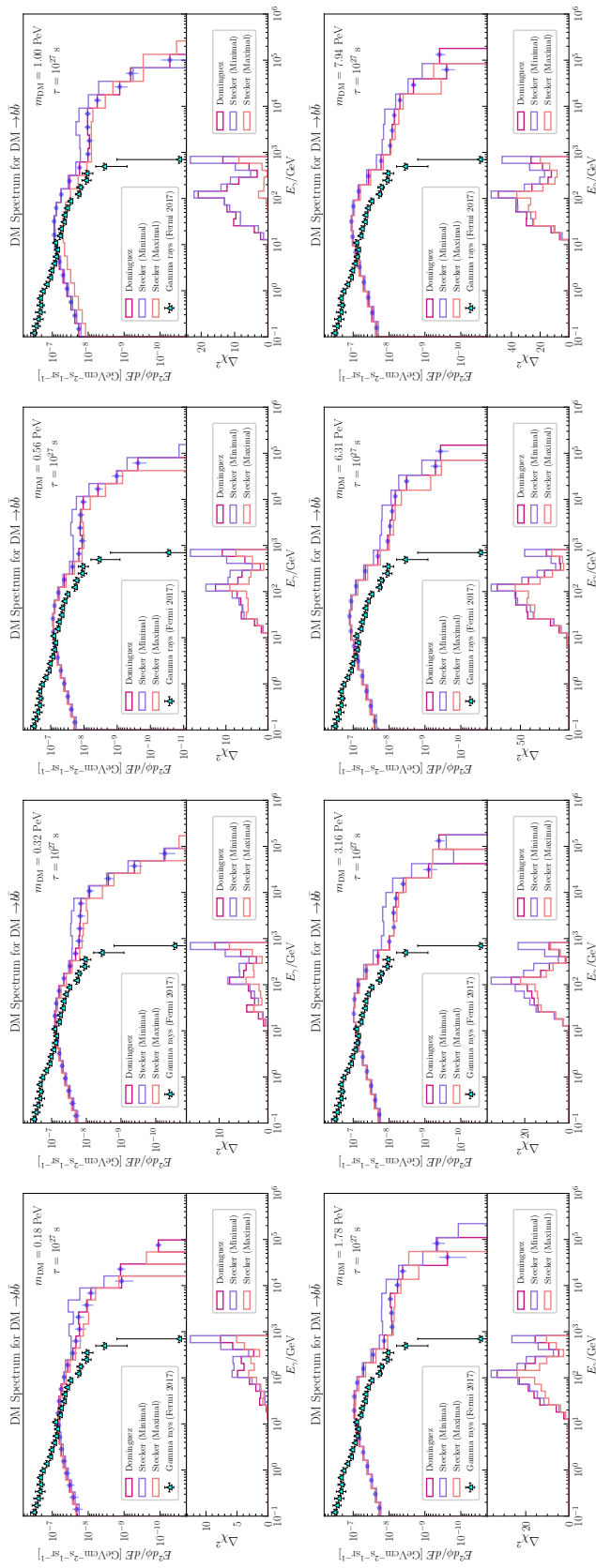


**Figure 9:** Final dark matter gamma-ray flux from the extragalactic secondary  $\gamma \rightarrow \gamma$  component, for different dark matter masses at a lifetime of  $10^{27}$  seconds. Different colors correspond to different EBL models considered for the propagation through the extragalactic space. The bottom panels show the  $\Delta\chi^2$  calculated by comparing our Monte Carlo simulations to Fermi-LAT measurements of the IGRB spectrum, displayed by the triangular points. The circular data points show the mean prediction and the corresponding errors from the Monte Carlo simulations according to the Dominguez *et al.* EBL model.

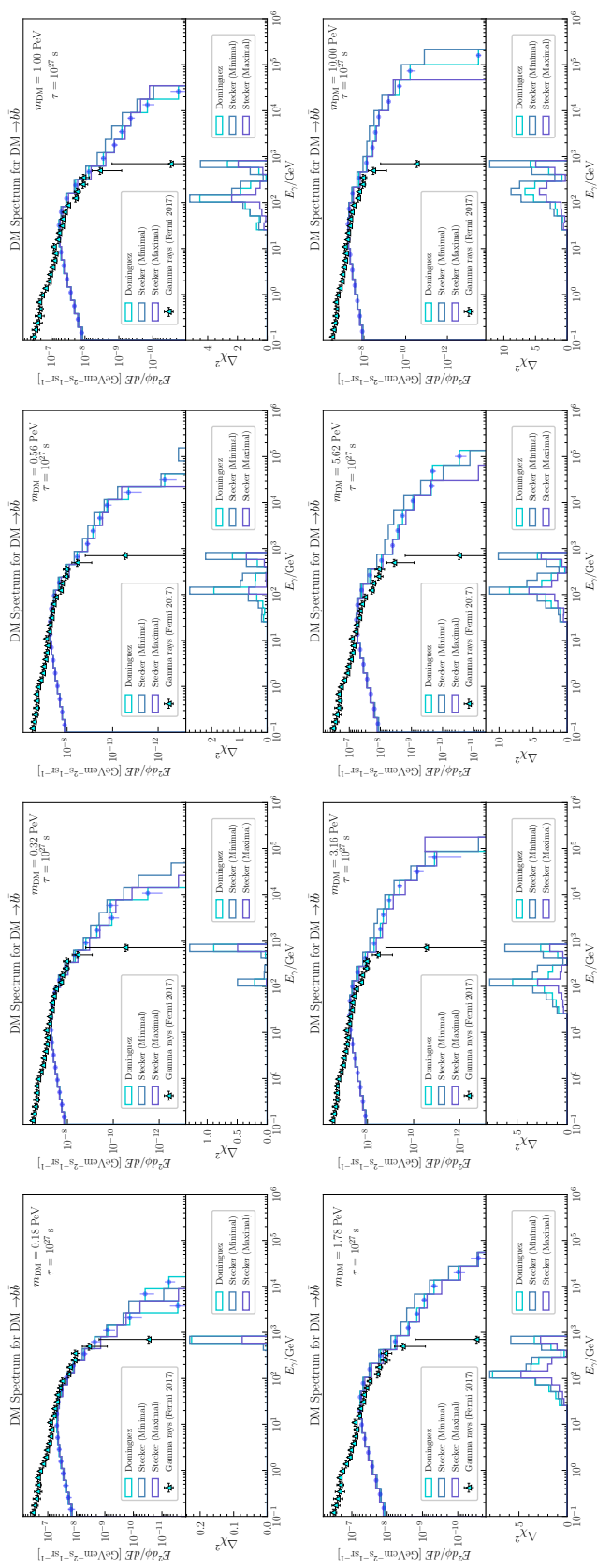


**Figure 10:** Final dark matter gamma-ray flux from the extragalactic secondary  $e^+e^- \rightarrow \gamma$  component, for different dark matter masses at a lifetime of  $10^{27}$  seconds. Different colors correspond to different EBL models considered for the propagation through the extragalactic space. The bottom panels show the  $\Delta\chi^2$  calculated by comparing our Monte Carlo simulations to Fermi-LAT measurements of the IGRB spectrum, displayed by the triangular points. The circular data points show the mean prediction and the corresponding errors from the Monte Carlo simulations according to the Dominguez *et al.* EBL model.